Nanoimprint Lithography-Directed Self-Assembly of Heterobimetallic FeM (M = Pd, Pt) Complexes for Magnetic Patterning

Zhengong Meng,[a,b] Guijun Li,[e] Sze-Chun Yiu,[a,c] Nianyong Zhu,[a] Zhen-Qiang Yu,*[b] Chi-Wah Leung,[f] Ian Manners[d] and Wai-Yeung Wong*[a,c]

[a] Dr. Z. Meng, Dr. S.-C. Yiu, Dr. N. Zhu, Prof. Dr. W.-Y. Wong
Department of Chemistry
Hong Kong Baptist University
Waterloo Road, Kowloon Tong, Hong Kong, P.R. China
E-mail: wai-yeung.wong@polyu.edu.hk

[b] Dr. Z. Meng, Prof. Dr. Z.-Q. Yu
College of Chemistry and Environmental Engineering
Low-dimensional Materials Genome Initiative, Shenzhen University
Xueyuan Road, Shenzhen, Guangdong, P.R. China
E-mail: zqyu@szu.edu.cn

[c] Prof. Dr. W.-Y. Wong
Department of Applied Biology and Chemical Technology
The Hong Kong Polytechnic University (PolyU)
Hung Hom, Hong Kong, P.R. China
PolyU Shenzhen Research Institute
Shenzhen, 518057, P.R. China
E-mail: wai-yeung.wong@polyu.edu.hk

[d] Prof. Dr. I. Manners
Department of Chemistry
University of Victoria
Victoria, BC V8P 5C2, Canada

[e] Dr. G. Li
State Key Laboratory of Ultra-Precision Machining Technology and Department of Industrial and Systems Engineering
The Hong Kong Polytechnic University
Hung Hom, Hong Kong, P.R. China

[f] Dr. C.-W. Leung
Department of Applied Physics
The Hong Kong Polytechnic University
Hung Hom, Hong Kong, P.R. China

Supporting information for this article is given via a link at the end of the document.

Abstract: Self-assembly of d^8 metal polypyridine systems is a well-established approach for the creation of 1D organometallic assemblies but there are still challenges for the large scale construction of nanostructured patterns from these building blocks. We describe here the use of high-throughput nanoimprint lithography (NIL) to direct the self-assembly of the heterobimetallic complexes [4′-ferrocenyl-(2,2′:6′,2″-terpyridine)M(OAc)]$^+$(OAc)$^-$ (M = Pd or Pt; OAc = acetate). Uniform nanorods are fabricated from the molecular self-organization and evidenced by morphological characterisation. More importantly, when top-down NIL is coupled with the bottom-up self-assembly of the organometallic building blocks, regular arrays of nanorods can be accessed and the patterns can be controlled by changing the lithographic stamp, where the mold imposes a confinement effect on the nanorod growth. In addition, patterns consisting of the products formed after pyrolysis are studied. The resulting arrays if ferromagnetic FeM alloy nanorods suggest promising potential for the scalable production of ordered magnetic arrays and fabrication of magnetic bit patterned media.

Introduction

Self-assembly has emerged as a highly effective bottom-up strategy for the construction of artificial architectures from simple building blocks, allowing precise control of otherwise randomly oriented molecules into highly ordered aggregates. Assemblies with increasing complexity in molecular packing often possess unique properties which offer potential in a variety of applications.[1] Within this field, metallosupramolecules formed by a weak driving force such as metal-ligand coordination, hydrogen bonding, or π-π interactions represent one of the most common building blocks to offer a bottom-up approach inspired by nature.[2]

Coordination compounds with a square-planar geometry have been of particular interest as precursors to construct supramolecular self-assembled systems due to the molecular π–π stacking and metal-metal interactions.[3] Self-assembly of these systems has attracted much attention because of the intriguing properties of the resulting assemblies, as well as the propensity to manipulate the structural ordering in organometallic compounds. Typically, N^N^N azole-based or polypyridyl ligand-based d^8 metal complexes have been well-known to exhibit a tendency towards stacking through weak non-covalent interactions.[4] The ligand is coordinated with diverse d^8 metal ions (such as Pt, Pd and Au, etc.) so as to facilitate the formation of stable square-planar structures, and the complexes show a strong tendency towards assembling into highly ordered aggregates with certain shape such as fibers, sheets, grids, cubes and wheels, etc.[5] Much progress on the supramolecular self-assembly of monometallic compounds has been achieved over the last few decades, however the construction of

This is the accepted version of the following article: Z. Meng, G. Li, S.-C. Yiu, N. Zhu, Z.-Q. Yu, C.-W. Leung, I. Manners, W.-Y. Wong, Angew. Chem. Int. Ed. 2020, 59, 11521, which has been published in final form at https://doi.org/10.1002/anie.202002685.

heterometallic extended architectures represents a significant challenge. The heterometallic block may furnish unprecedented morphologies and unique functions in the tailored assemblies because of the intrinsic synergistic effect between different metals, thus offering potential for numerous technological applications.[6]

In our recent work a ferrocenyl-functionalized polypyridyl ligand (Fc-TPy) has been coordinated by d^8-metal ions to form unique square-planar complexes, where the ferrocene (Fc) group as a pendant can fill the stacking space and further enhance the intermolecular interactions.[7] The introduction of ferrocene in polypyridyl ligands leads to particularly interesting behavior in a heterobimetallic system after metal ion coordination.[8] With respect to redox switching, the Fc unit shows the reversible Fc/Fc^+ couple for electroactive nanoarchitectures and switchable anticancer activity has also been reported.[8c,9] For the synthesis of Fe-based ferromagnetic alloy nanoparticles (NPs), the weak interactions among the molecular precursors enable the formation of ordered aggregates which further ensure the uniformity of NPs.[7] Besides providing the rich functionality, the sterically bulky pendant has also been shown not to affect the intramolecular interactions, but to favor the stacking behavior in a head-to-tail mode.[7a] Following this principle and our previous research work on the synthesis and patterning of FePt NPs, it would be intriguing to develop the Fc-TPy system for heterobimetallic self-assembly.

The aggregates formed by bottom-up self-assembly often possess uniform molecular order but this remains difficult to prepare the precise patterns in a large scale. In contrast, the top-down method of nanoimprint lithography (NIL) provides a feasible approach to establish an ideal solution-processable technique for mass production with high throughput.[7b,10] In this method, the imprinted regular features can be observed, but the molecular arrangement on the lithographic lengthscale is also difficult to control. For this reason, the combination of self-assembly and NIL offers the possibility of effectively achieving the goal of patterning the assemblies, especially in the case of *in-situ* self-assembly within the features of the template.[11] This may promote the application of assemblies in device fabrication and further optimize their efficiency.[12] In this respect, as previous reports on the patterning of magnetic NPs using block copolymers led to dot arrays as separate magnetic islands in bit-patterned media,[13] the introduction of soft lithographic methods should further help to achieve the goal of patterning the assemblies.[14]

Inspired by the well-established self-assembly of square-planar Pt(II) and Pd(II) complexes,[15] we further exploited this approach to construct nanoarchitectures based on heterobimetallic complexes, and also demonstrate how assembled bimetallic complexes can be orderly patterned in bulk to furnish magnetic recording media through a combination with NIL. To achieve our aim, we prepared two cationic bimetallic complexes, namely **Fc-TPyM** (M = Pt or Pd), where the typical terpyridine ligand for coordinating d^8 metal ions is introduced to favor the common M···M and π-π stacking interactions. These complexes are expected to exhibit a strong tendency to aggregate, and are shown to further self-assemble into highly oriented arrays of nanorods along lithographic features which, upon pyrolysis, afford ferromagnetic FeM alloy nanorods while maintaining the same periodicity. The potential of the latter in magnetic recording media is highlighted in the magnetic force microscope (MFM) images.

Results and Discussion

Molecular design and characterization

In our synthetic design, the tridentate ligand of 4′-(ferrocenyl)-[2,2′:6′,2″]terpyridine was synthesized and the terpyridine unit was used to provide coordination site for metal ions. The synthetic routes are shown in Scheme S1. The heterobimetallic complex **Fc-TPyPd** was obtained by directly coordinating the ligand with $Pd(OAc)_2$ (OAc = acetate) and the substitution of chloride in **Fc-TPyPt-Cl** with AgOAc gave **Fc-TPyPt**. The introduction of acetyl group was utilized to increase the intermolecular interactions due to the H-bonding apart from the M···M and π-π stacking interactions.

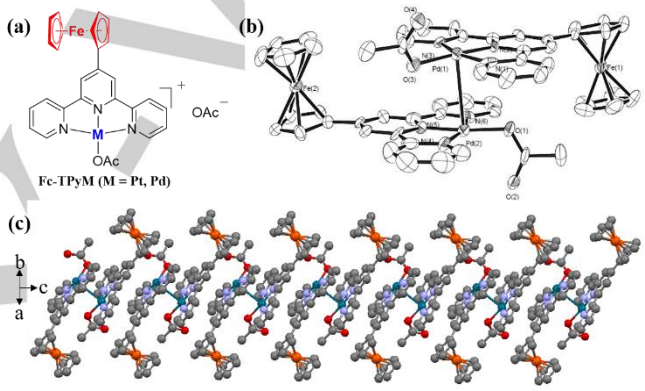

Figure 1. (a) Chemical structure of heterobimetallic complexes **Fc-TPyM** (M = Pt, Pd); (b) An ORTEP view of **Fc-TPyPd** and the partial atom numbering scheme; (c) Illustrations of the π-π stacking and Pd···Pd interactions in the molecular structure along the *c*-axis. The H-atoms are not shown for clarity.

High quality crystals of **Fc-TPyPd** were grown by slow vapor diffusion of Et_2O into a MeCN (acetonitrile) solution of the complex, and the molecular structure in the solid state was established by X-ray crystallography. The corresponding metric parameters, selected bond lengths and angles are given in Tables S1 and S2, respectively. The space group of **Fc-TPyPd** is $P2_12_12$ with a formula of [4′-ferrocenyl-(2,2′:6′,2″-terpyridine)Pd(OAc)]$^+$ for the cation. As shown in Figure 1b, the Pd ion binds tightly to the three adjacent pyridyl N sites and an irregular coplanar motif is formed. Also, a dimeric packing motif was observed with a Pd···Pd distance of 3.17 Å and adjacent molecules stacked on top of each other in a head-to-tail fashion, while the ferrocenyl groups in the two adjacent molecules were located in the opposite directions. Besides, the cationic Pd(II) molecules formed separate columnar stacking parallel to the *c*-axis (Figure 1c) owing to their π-π stacking between the coplanar terpyridine moieties, resulting in the torsion angle of Pd···Pd···Pd to be 123.41° and the interplanar distance to be 3.10 Å. The side view along the crystallographic c axis is shown in Fig. S1, and clear channels were observed to further indicate their ordered intermolecular stacking. The planar structure and the suitable distance of two adjacent π-planes further give the intermolecular interactions suitable for self-assembly, including

the π-π stacking and intermetallic interactions, etc. Furthermore, the intermolecular metal-metal-to-ligand charge transfer (MMLCT) and intraligand transitions in solution were also established from their UV absorption spectra (Figure S2) to instrumentally explain the potency in the stacking behavior. Empirically, the intermolecular distance in the range of 3.0-3.5 Å usually brings about the axial interaction with π-π stacking and metal···metal orbital overlap. The close interaction gives rise to the possible transitions with the MMLCT nature. The broad peak from the ferrocenyl pendant was obviously shifted from 460 nm to over 600 nm after coordination with the metal center, and the shoulder peak appearing at 375 nm for **Fc-TPyPd** could be ascribed to the metallophilic Pd···Pd interaction. The twin plot for **Fc-TPyPt** with respect to **Fc-TPyPd** was observed with an obvious redshift and implied the same type of MMLCT transitions.

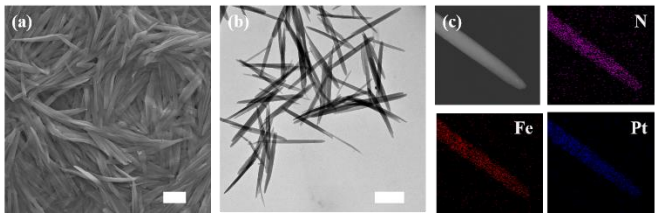

Figure 2. (a) SEM image and (b) TEM image of the self-assembled nanorods prepared from the **Fc-TPyPt** solution of hexane/$CHCl_3$ (v/v = 4/6) after aging for 15 min; (c) STEM image and the corresponding elemental mapping images for N, Fe and Pt atoms. Scale bar: 1 μm.

Kinetic control of self-assembly

In this bimetallic system, the introduction of the sterically bulky ferrocene did not prevent the square planar geometry of the terpyridine complexes from favoring the formation of aggregates mediated by the intermolecular interactions. As a consequence, the saturated solution of **Fc-TPyM** in $CHCl_3$ easily self-assembled to give a precipitate, and the morphology of the resulting aggregates was observed and is shown in Figure S3. The overall aggregate was amorphous, but part of the nanorods was clearly observed in scanning electron microscope (SEM) presumably due to the stronger M···M interactions in **Fc-TPyPt** than that in **Fc-TPyPd**.

To further gain the deeper insight into the self-assembly process of such bimetallic complexes, the kinetic equilibrium of **Fc-TPyPt** in solvent/non-solvent mixtures with controllable ratios was systematically studied. In view of the solubility in good solvent and the miscibility of two solvents, the mixture was chosen as $CHCl_3$:hexane and a wide range of ratios was used. For the specific volume ratio of 50:50 ($CHCl_3$:hexane), 0.4 mL of $CHCl_3$ and 0.5 mL of hexane was mixed uniformly, and then 0.1 mL of the solution of **Fc-TPyPt** in $CHCl_3$ (10^{-3} M) was rapidly injected into the solvent mixture, the mixture was aged until the dynamic equilibrium was reached. The equilibrium with a faster aging process was reached upon increasing the hexane content, but the rapid rate was identified to favor precipitation and not suitable for ordered molecular arrangements. The aggregates were obtained in the mixture when its ratio of $CHCl_3$:hexane was 50:50, and the SEM image in Figure S4 presents the agglomeration state on a large lengthscale comprising many separated nanorods. The ratio of $CHCl_3$:hexane was further optimized at 40:60 to give highly ordered and monodisperse rods in the aging process. The SEM and transmission electron microscope (TEM) images in Figure 2 show the uniform shape of rods with an average length of 2 μm, and TEM-elemental mapping of the molecular assemblies demonstrated the homogeneous distribution of elemental N, Pt and Fe, suggesting the bimetallic composition of Fe,Pt-based organometallic rods (Figure 2c). Thus, the **Fc-TPyPt** complex exhibited an interesting metallophilic assembly process during the kinetic crystallization process, and then the crystallization-driven self-assembly (CDSA) was further accompanied by the growth of rods .

Nanoimprint lithography-directed self-assembly

Although the creation of uniform architectures from the bottom-up self-assembly is fascinating owing to the weak supramolecular interactions, achieving the regular orientation of the molecular assemblies is important for realizing their potential. Ultimately driven by the metallophilic interactions and π-π stacking forces between adjacent molecules, the heterometallic complexes of **Fc-TPyM** could serve as novel building blocks to construct more functional structures with the subtle molecular control. The self-assembled rods were obtained by kinetically controlling the process of crystallization, but to fulfill their real promise control over their dispersion on a substrate was required.

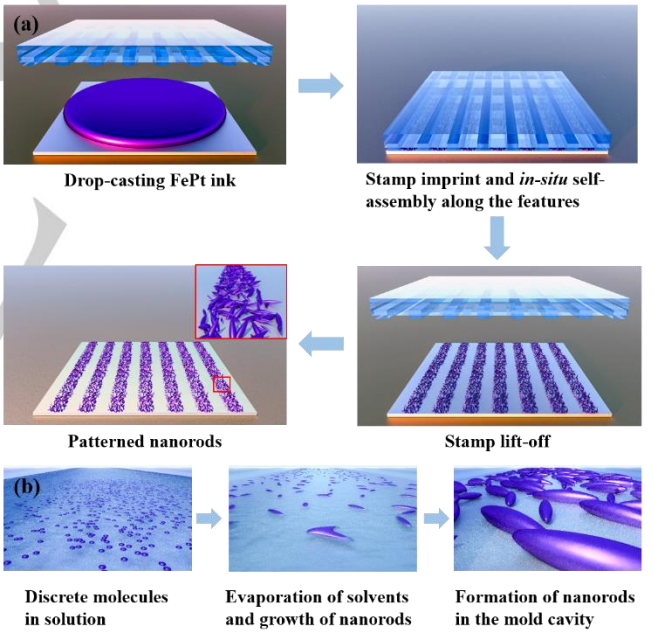

Figure 3. (a) Illustration of the lithographic process of self-assembly: the chloroform solution of **Fc-TPyPt** as ink is drop-cast onto the substrate, and then the PDMS stamp is pressed onto the sample; *In-situ* self-assembly is promoted along the features of the PDMS template and the self-assembled nanorods are being patterned; the stamp is then lifted off and the patterned assemblies are left along the features. Inset: the enlarged view of the selected area. (b) a cartoon representation of the formation of nanorods in the mold cavity.

Lithographic patterning was identified as an efficient approach to prepare ordered functional features on a large scale, and the strategy of integrating bottom-up self-assembly and top-down NIL was explored here to direct the orientation of the assembled

nanostructures and the building of ordered patterns on certain substrates. As illustrated in Figure 3a, the chloroform solution of **Fc-TPyPt** (10^{-3} M) was drop-cast onto a silicon substrate, and then a featured poly(dimethylsiloxane) (PDMS) template was cast to control the slow evaporation of the solvents and promote molecular self-organization in the mold cavity; Finally, the assemblies were patterned along the feature of the template. In addition, a cartoon representation in Figure 3b was used to clearly illustrate the formation of nanorods in the mold cavity. Initially, the molecules were discrete and freely dispersed in solution. The solvents were evaporated slowly during the stamping process, and the nanorods grew gradually to provide the final patterned nanorods along the features. When there were no features in the templates, the patterns obtained were only formed by the molecular self-assembly and characterized by SEM and atomic force microscopy (AFM), as shown in Figures 4a and 4e, and the images indicate that the monodisperse rod-like arrays were formed with the mean height of 30 nm, but there was no fixed orientation. On this basis, PDMS stamps with ordered line or hexagonal arrays were further introduced, and then the material was assembled along the features of the templates, Figures 4b-d give clear patterns of nanorods along the templates' features and identify the feasibility of controlling the orientation by NIL. The length of the rods is decreased to about 300 nm after introducing the lithographic process, which is considerably shorter than that of the assembled rods in solvent/non-solvent media; Also, the length of less than 200 nm is further shortened in the line or hexagonal arrays. This can be attributed to a confinement effect, in which the soft templates effectively fix the solution into their features to offer a limited space for self-assembly, and the growth of the rods can only proceed along the confined features of the templates. Overall, the soft lithography and self-assembly were nicely combined to prepare the organometallic patterns successfully, and provided a high throughput method for orienting the assembled architectures.

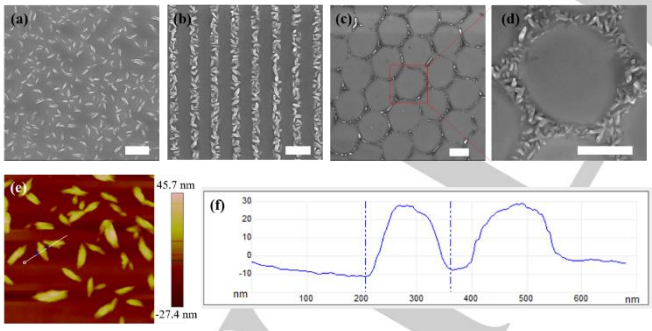

Figure 4. The self-assembled nanorods derived from **Fc-TPyPt** are patterned using NIL: SEM images of (a) disordered patterns, (b) line-oriented patterns, (c) hexagonal patterns and (d) amplified hexagonal patterns; scale bar: 1 μm. (e) AFM image and (f) cross-section analysis displaying the height profile of the self-assembled patterns; size: 2×2 μm^2.

Fe,Pt-containing bimetallic complexes were identified as single-source precursors from which to prepare magnetic FePt alloy NPs by one-step pyrolysis, and to fabricate ordered patterns with ultra-high density for magnetic recording media. Herein, **Fc-TPyPt** served as a single-source precursor to FePt NPs. The characterization data in Figure S5 show the spherical morphology, $L1_0$ phase and ferromagnetic hysteresis loop, etc of these NPs. This set of pyrolytic conditions was also deployed for the pyrolysis of the self-assembled rods of **Fc-TPyPt** at 800 ℃ for 1 h under an Ar/H_2 (95/5) atmosphere, and then Fe and Pt were allowed to form ferromagnetic FePt rods with the collapse of the organic frameworks. As expected, the pyrolyzed patterns were observed in Figure 5a and 5b. The features and morphology were also kept the same as before, but the height of the nanorods in Figure 5b compared to that in Figure 4e was decreased from 30 nm to 10 nm due to the collapse of the organic skeleton according to the AFM images. In addition, the magnetic behavior was also studied by MFM, as indicated in Figure 5c and 5f, and the distinct magnetic signal corresponding to the related AFM images was detected, which implied the strong magnetic properties of the NIL-directed assemblies.

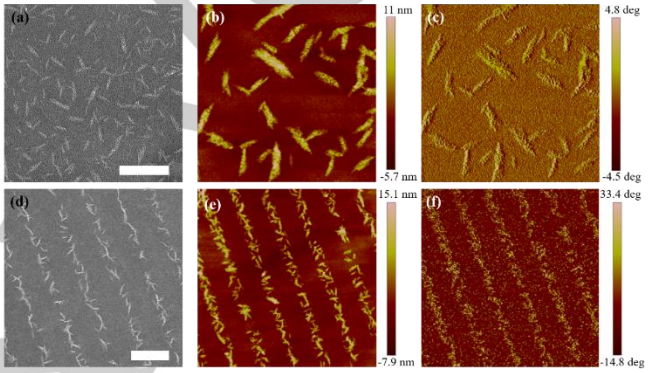

Figure 5. Magnetic patterns of FePt alloy NPs derived from the pyrolysis of the self-assembled nanorods of **Fc-TPyPt**: SEM images in (a) and (d) of the magnetic patterns corresponding to Figure 4a and 4b, respectively; scale bar: 1 μm. (b) and (e): AFM images of the patterns; (c) and (f): MFM images related to (b) and (e), respectively; size: 2×2 μm^2 for (b) and (c); 5×5 μm^2 for (e) and (f).

The other bimetallic complex, **Fc-TPyPd,** also showed significant π–π stacking and metallophilic interactions, and easily aggregated in the solid state or concentrated solution. However, the intermolecular Pd···Pd interaction is significantly weaker than the Pt···Pt case, such that the lithographic self-assembly of **Fc-TPyPd** cannot be achieved directly. Hence, a subtle design was explored to assist the process by introducing a linear polystyrene (**PS**). The chloroform solution of **TPy-FePd** and **PS** (10^{-3} M, 7:3 in mole ratio) was used as the substituents to achieve the assembled patterns. As shown in Figure S8a, the morphology of **PS** nanospheres together with **TPy-FePd** nanorods was observed by SEM analysis. The nanorods had an average length of 250 nm and were evenly dispersed around the **PS** spheres. Besides, the introduction of the line features also afforded the alternate **PS** line arrays and FePd metallic rods along the line orientation (Figure S8d). **TPy-FePd** was also identified as a good candidate for preparing ferromagnetic FePd alloy NPs, and Figure S6 shows the characterization of the resultant FePd NPs in detail. The NPs exhibited excellent ferromagnetic behavior with a high coercivity of 4.9 kOe and were evenly dispersed in the carbon matrix with the mean size of 16.2 nm. Then the substrate was subject to pyrolysis by the same conditions as in the preparation of ferromagnetic FePd NPs. As shown in the SEM image (Figure S8b), all the PS

spheres were removed after pyrolysis, and only magnetic FePd alloy NPs were left on the substrate, which still kept their original shapes of the nanorods but with a skeletal collapse. The AFM image in Figure S8c further indicates the morphology of the pyrolyzed nanorods and the decreased height. Also, the line-oriented FePd nanorods were pyrolyzed to present the resultant ferromagnetic patterns in a grating array. The XPS spectra of Fe 2p and Pd 3d in Figure S9 further supported the formation of FePd alloy NPs.

Conclusion

Ferrocene-based terpyridine was used to coordinate with d^8 metal ions to form two cationic heterobimetallic complexes Fc-TPyM (M = Pt, Pd) with intermolecular π-π stacking and M···M interactions. The self-assembly of the complexes was investigated in a solvent/non-solvent system to reveal the dynamic equilibrium to prepare highly ordered rod-like heterobimetallic architectures. We further promoted the development of patterning the assemblies by combining the bottom-up self-assembly and the top-down NIL. Precise control of the orientation of the assemblies was realized along the lithographic features, and the morphology corresponding to magnetic islands of the oriented assemblies was retained on pyrolysis to suggest potential for the approach in magnetic data recording. As demonstrated here for the lithography-induced self-assembly, it is possible to contemplate the mass production of the ordered arrays of the assemblies in a large scale by exploiting the high throughput NIL protocol.

Acknowledgements

This work was supported by the Science, Technology and Innovation Committee of Shenzhen Municipality (JCYJ20180507183413211), the National Natural Science Foundation of China (51873176 and 21701112), the Hong Kong Research Grants Council (PolyU153062/18P), the Hong Kong Polytechnic University (1-ZE1C) and Ms Clarea Au for the Endowed Professorship in Energy (847S). Special thanks were also given to Instrumental Analysis Center of Shenzhen University (Xili Campus). Ian Manners thanks the Canadian Government for a Canada 150 Research Chair.

Keywords: Heterobimetallic complexes • self-assembly • nanoimprint lithography • nanorods • magnetic FePt nanoparticles

[1] a) R. Aoki, R. Toyoda, J. F. Kogel, R. Sakamoto, J. Kumar, Y. Kitagawa, K. Harano, T. Kawai, H. Nishihara, *J. Am. Chem. Soc.* **2017**, *139*, 16024-16027; b) X. M. He, M. S. Hsiao, C. E. Boott, R. L. Harniman, A. Nazemi, X. Y. Li, M. A. Winnik, I. Manners, *Nat. Mater.* **2017**, *16*, 481-488; c) B. Song, S. Kandapal, J. L. Gu, K. R. Zhang, A. Reese, Y. F. Ying, L. Wang, H. Wang, Y. M. Li, M. Wang, S. Lu, X. Q. Hao, X. H. Li, B. Q. Xu, X. P. Li, *Nat. Commun.* **2018**, *9*, 4575; d) J. M. Lehn, *Science* **2002**, *295*, 2400-2403.

[2] a) P. F. Wei, X. Z. Yan, F. H. Huang, *Chem. Soc. Rev.* **2015**, *44*, 815-832; b) X. Z. Yan, T. R. Cook, P. Wang, F. H. Huang, P. J. Stang, *Nat. Chem.* **2015**, *7*, 342-348; c) G. R. Whittell, M. D. Hager, U. S. Schubert, I. Manners, *Nat. Mater.* **2011**, *10*, 176-188; d) J. H. Tang, Y. Sun, Z. L. Gong, Z. Y. Li, Z. X. Zhou, H. Wang, X. P. Li, M. L. Saha, Y. W. Zhong, P. J. Stang, *J. Am. Chem. Soc.* **2018**, *140*, 7723-7729.

[3] a) I. Eryazici, C. N. Moorefield, G. R. Newkome, *Chem. Rev.* **2008**, *108*, 1834-1895; b) Y. Ai, M. H. Y. Chan, A. K. W. Chan, M. Ng, Y. G. Li, V. W. W. Yam, *Proc. Natl. Acad. Sci. USA* **2019**, *116*, 13856-13861; c) A. Aliprandi, M. Mauro, L. De Cola, *Nat. Chem.* **2016**, ***8***, 10-15.

[4] a) M. Mauro, A. Aliprandi, D. Septiadi, N. S. Kehra, L. De Cola, *Chem. Soc. Rev.* **2014**, *43*, 4144-4166; b) A. Winter, S. Hoeppener, G. R. Natikome, U. S. Schubert, *Adv. Mater.* **2011**, *23*, 3484-3498.

[5] a) H. L. Au-Yeung, S. Y. L. Leung, A. Y. Y. Tam, V. W. W. Yam, *J. Am. Chem. Soc.* **2014**, *136*, 17910-17913; b) C. Y. S. Chung, V. W. W. Yam, *J. Am. Chem. Soc.* **2011**, *133*, 18775-18784; c) Y. Chen, K. Li, W. Lu, S. S. Y. Chui, C. W. Ma, C. M. Che, *Angew. Chem. Int. Ed.* **2009**, *48*, 9909-9913; d) W. Lu, S. S. Y. Chui, K. M. Ng, C. M. Che, *Angew. Chem. Int. Ed.* **2008**, *47*, 4568-4572.

[6] a) M. El Garah, N. Marets, M. Mauro, A. Aliprandi, S. Bonacchi, L. De Cola, A. Ciesielski, V. Bulach, M. W. Hosseini, P. Samori, *J. Am. Chem. Soc.* **2015**, *137*, 8450-8459; b) S. Chakraborty, W. Hong, K. J. Endres, T. Z. Xie, L. Wojtas, C. N. Moorefield, C. Wesdemiotis, G. R. Newkome, *J. Am. Chem. Soc.* **2017**, *139*, 3012-3020.

[7] a) Z. G. Meng, C. L. Ho, H. F. Wong, Z. Q. Yu, N. Y. Zhu, G. J. Li, C. W. Leung, W.-Y. Wong, *Sci. China Mater.* **2019**, *62*, 566-576; b) Q. C. Dong, Z. G. Meng, C. L. Ho, H. G. Guo, W. Y. Yang, I. Manners, L. L. Xu, W.-Y. Wong, *Chem. Soc. Rev.* **2018**, *47*, 4934-4953.

[8] a) L. Xu, Y. X. Wang, L. J. Chen, H. B. Yang, *Chem. Soc. Rev.* **2015**, *44*, 2148-2167; b) L. B. Xing, S. Yu, X. J. Wang, G. X. Wang, B. Chen, L. P. Zhang, C. H. Tung, L. Z. Wu, *Chem. Commun.* **2012**, *48*, 10886-10888; c) K. Mitra, A. Shettar, P. Kondaiah, A. R. Chakravarty, *Inorg. Chem.* **2016**, *55*, 5612-5622; d) K. Mitra, U. Basu, I. Khan, B. Maity, P. Kondaiah, A. R. Chakravarty, *Dalton Trans.* **2014**, *43*, 751-763

[9] a) D. Astruc, *Eur. J. Inorg. Chem.* **2017**, 6–29; b) M. S. Inkpen, S. Scheerer, M. Linseis, A. J. P. White, R. F. Winter, T. Albrecht, N. J. Long, *Nat. Chem.* **2016**, *8*, 825–830; d) L. E. Wilson, C. Hassenruck, R. F. Winter, A. J. P. White, T. Albrecht, N. J. Long, *Angew. Chem. Int. Ed.* **2017**, *56*, 6838-6842.

[10] M. C. Denis Gentili, *Coord. Chem. Rev.* **2013**, *257*, 2456-2467.

[11] a) J. A. Liddle, Y. Cui, P. Alivisatos, *J. Vac. Sci. Technol. B* **2004**, *22*, 3409-3414; b) J. K. Bosworth, M. Y. Paik, R. Ruiz, E. L. Schwartz, J. Q. Huang, A. W. Ko, D. M. Smilgies, C. T. Black, C. K. Ober, *ACS Nano* **2008**, *2*, 1396-1402; c) S. C. G. Molnár, J. A. Real, F. Carcenac, E. Daran, C. Vieu, A. Bousseksou, *Adv. Mater.* **2007**, *19*, 2163-2167.

[12] a) H. U. Jeon, H. M. Jin, J. Y. Kim, S. K. Cha, J. H. Mun, K. E. Lee, J. J. Oh, T. Yun, J. S. Kim, S. O. Kim, *Mol. Syst. Des. Eng.* **2017**, *2*, 560-566; b) Z. Y. Wang, T. Liu, Y. Yu, M. Asif, N. Xu, F. Xiao, H. F. Liu, *Small* **2018**, *14*, 1802670; c) Y. Zhou, Y. Shi, F. B. Wang, X. H. Xia, *Anal. Chem.* **2019**, *91*, 2759-2767; d) Y. Ma, P. She, S. Liu, L. Shen, X. Li, S. Liu, Q. Zhao, W. Huang, W.-Y. Wong, *Small Methods* **2019**, *3*, 1900142.

[13] a) S. C. Yiu, A. Nunns, C. L. Ho, J. H. L. Ngai, Z. G. Meng, G. J. Li, J. Gwyther, G. R. Whittell, I. Manners, W.-Y. Wong, *Macromolecules* **2019**, *52*, 3176-3186; b) B. Basly, T. Alnasser, K. Aissou, G. Fleury, G. Pecastaings, G. Hadziioannou, E. Duguet, G. Goglio, S. Mornet, *Langmuir* **2015**, *31*, 6675-6680.

[14] a) G. W. Yang, G. P. Wu, X. X. Chen, S. S. Xiong, C. G. Arges, S. X. Ji, P. F. Nealey, X. B. Lu, D. J. Darensbourg, Z. K. Xu, *Nano Lett.* **2017**, *17*, 1233-1239; b) X. Y. Liu, N. Bhandaru, M. Banik, X. T. Wang, A. M. Al-Enizi, A. Karim, R. Mukherjee, *ACS Omega* **2018**, *3*, 2161-2168.

[15] a) Y. Chen, C. M. Che, W. Lu, *Chem. Commun.* **2015**, *51*, 5371-5374; b) J. Wang, L. J. Li, W. L. Yang, Z. H. Yan, Y. F. Zhou, B. H. Wang, B. Zhang, W. F. Bu, *ACS Macro Lett.* **2019**, *8*, 1012-1016; c) Z. L. Gong, Y. W. Zhong, J. N. Yao, *J. Mater. Chem. C* **2017**, *5*, 7222-7229; d) Y. S. Wong, F. C. M. Leung, M. Ng, H. K. Cheng, V. W. W. Yam, *Angew. Chem. Int. Ed.* **2018**, *57*, 15797-15801.

Entry for the Table of Contents

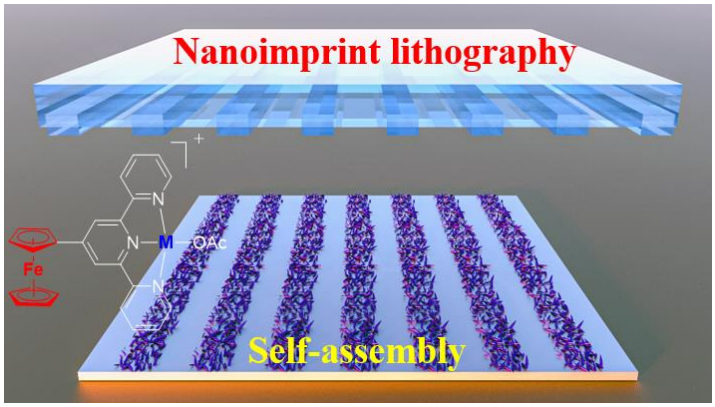

When the top-down lithography is coupled with the bottom-up self-assembly, the molecular self-assembly of heterobimetallic complexes can be precisely controlled to prepare ordered patterns of assemblies with high throughput.